H2O at the Phoenix Landing Site

P. H. Smith, *et al.*

Science **325**, 58 (2009);
DOI: 10.1126/science.1172339

21. B. U. Forstmann, M. Brass, I. Koch, D. Y. von Cramon, *Neuropsychologia* **43**, 943 (2005).
22. S. L. Bengtsson, J. D. Haynes, K. Sakai, M. J. Buckley, R. E. Passingham, *Cereb. Cortex* (2009).
23. J. B. Rowe, K. E. Stephan, K. Friston, R. S. J. Frackowiak, R. E. Passingham, *Cereb. Cortex* **15**, 85 (2005).
24. M. R. Roesch, C. R. Olson, *J. Neurophysiol.* **90**, 1766 (2003).
25. L. Tremblay, W. Schultz, *Nature* **398**, 704 (1999).
26. M. R. Roesch, C. R. Olson, *Science* **304**, 307 (2004).
27. C. Padoa-Schioppa, J. A. Assad, *Nature* **441**, 223 (2006).
28. C. Padoa-Schioppa, J. A. Assad, *Nat. Neurosci.* **11**, 95 (2008).
29. A. Izquierdo, R. K. Suda, E. A. Murray, *J. Neurosci.* **24**, 7540 (2004).
30. C. M. Butter, *Physiol. Behav.* **4**, 163 (1969).
31. C. M. Butter, M. Mishkin, H. E. Rosvold, *Exp. Neurol.* **7**, 65 (1963).
32. K. Shima, J. Tanji, *Science* **282**, 1335 (1998).
33. S. W. Kennerley, M. E. Walton, T. E. J. Behrens, M. J. Buckley, M. F. S. Rushworth, *Nat. Neurosci.* **9**, 940 (2006).
34. P. H. Rudebeck *et al.*, *J. Neurosci.* **28**, 13775 (2008).
35. P. H. Rudebeck, E. A. Murray, *J. Neurosci.* **28**, 8338 (2008).
36. P. H. Rudebeck, M. J. Buckley, M. E. Walton, M. F. S. Rushworth, *Science* **313**, 1310 (2006).
37. Materials and methods are available as supporting material on *Science* Online.
38. M. F. S. Rushworth, P. D. Nixon, M. J. Eacott, R. E. Passingham, *J. Neurosci.* **17**, 4829 (1997).
39. M. Mishkin, F. J. Manning, *Brain Res.* **143**, 313 (1978).
40. R. Passingham, *Brain Res.* **92**, 89 (1975).
41. S. T. Carmichael, J. L. Price, *J. Comp. Neurol.* **363**, 642 (1995).
42. M. J. Webster, J. Bachevalier, L. G. Ungerleider, *Cereb. Cortex* **4**, 470 (1994).
43. N. D. Daw, Y. Niv, P. Dayan, *Nat. Neurosci.* **8**, 1704 (2005).
44. E. K. Miller, T. J. Buschman, in *Neuroscience of Rule-Guided Behavior*, S. A. Bunge, J. D. Wallis, Eds. (Oxford Univ. Press, New York, 2008), pp. 419–440.
45. S. P. Wise, E. A. Murray, C. R. Gerfen, *Crit. Rev. Neurobiol.* **10**, 317 (1996).
46. M. J. Buckley, D. Gaffan, *Trends Cogn. Sci.* **10**, 100 (2006).
47. K. Tanaka, *Annu. Rev. Neurosci.* **19**, 109 (1996).
48. R. Dias, T. W. Robbins, A. C. Roberts, *Nature* **380**, 69 (1996).
49. T. L. Moore, S. P. Schettler, R. J. Killiany, D. L. Rosene, M. B. Moss, *Behav. Neurosci.* **123**, 231 (2009).
50. Y. Chudasama, J. D. Kralik, E. A. Murray, *Cereb. Cortex* **17**, 1154 (2006).
51. M. F. S. Rushworth, M. E. Walton, S. W. Kennerley, D. M. Bannerman, *Trends Cogn. Sci.* **8**, 410 (2004).
52. K. A. Hadland, M. F. S. Rushworth, D. Gaffan, R. E. Passingham, *J. Neurophysiol.* **89**, 1161 (2003).
53. M. M. Botvinick, T. S. Braver, D. M. Barch, C. S. Carter, J. D. Cohen, *Psychol. Rev.* **108**, 624 (2001).
54. F. A. Mansouri, M. J. Buckley, K. Tanaka, *Science* **318**, 987 (2007).
55. M. F. S. Rushworth, T. E. J. Behrens, *Nat. Neurosci.* **11**, 389 (2008).
56. M. R. Roesch, A. R. Taylor, G. Schoenbaum, *Neuron* **51**, 509 (2006).
57. M. E. Walton, D. M. Bannerman, K. Alterescu, M. F. S. Rushworth, *J. Neurosci.* **23**, 6475 (2003).
58. T. E. J. Behrens, M. W. Woolrich, M. E. Walton, M. F. S. Rushworth, *Nat. Neurosci.* **10**, 1214 (2007).
59. F. A. Mansouri, K. Tanaka, M. J. Buckley, *Nat. Rev. Neurosci.* **10**, 141 (2009).
60. M. Petrides, *J. Neurosci.* **15**, 359 (1995).
61. D. Gaffan, *Philos. Trans. R. Soc. London Ser. B Biol. Sci.* **357**, 1111 (2002).
62. P. W. Burgess, E. Veitch, A. D. Costello, T. Shallice, *Neuropsychologia* **38**, 848 (2000).
63. D. Badre, J. Hoffman, J. W. Cooney, M. D'Esposito, *Nat. Neurosci.* **12**, 515 (2009).
64. D. Badre, *Trends Cogn. Sci.* **12**, 193 (2008).
65. E. Koechlin, A. Hyafil, *Science* **318**, 594 (2007).
66. P. W. Burgess, S. J. Gilbert, I. Dumontheil, *Philos. Trans. R. Soc. London B Biol. Sci.* **362**, 887 (2007).

67. This research was jointly supported by a Royal Society University Research Fellowship (M.J.B.), a U.K. Medical Research Council (MRC) project grant (M.J.B.), a grant-in-aid for Scientific Research on Priority Areas from the Ministry of Education, Culture, Sports, Science, and Technology of Japan (K.T.), and an MRC program grant held by D. Gaffan, whom we thank for encouragement and support. We also wish to thank M. G. Baxter for assistance with anesthesia, and G. J. Daubney, K. Rockland, N. Ichinohe, H. Mashiko, and Y. Abe for assistance in preparing tissues for histology.

Supporting Online Material

www.sciencemag.org/cgi/content/full/325/5936/52/DC1
Materials and Methods
SOM Text
Figs. S1 to S6
References

17 February 2009; accepted 26 May 2009
10.1126/science.1172377

REPORTS

H_2O at the Phoenix Landing Site

P. H. Smith,[1]* L. K. Tamppari,[2] R. E. Arvidson,[3] D. Bass,[2] D. Blaney,[2] W. V. Boynton,[1] A. Carswell,[4] D. C. Catling,[5] B. C. Clark,[6] T. Duck,[7] E. DeJong,[2] D. Fisher,[8] W. Goetz,[9] H. P. Gunnlaugsson,[10] M. H. Hecht,[2] V. Hipkin,[11] J. Hoffman,[12] S. F. Hviid,[9] H. U. Keller,[9] S. P. Kounaves,[13] C. F. Lange,[14] M. T. Lemmon,[15] M. B. Madsen,[16] W. J. Markiewicz,[9] J. Marshall,[17] C. P. McKay,[18] M. T. Mellon,[19] D. W. Ming,[20] R. V. Morris,[20] W. T. Pike,[21] N. Renno,[22] U. Staufer,[23] C. Stoker,[18] P. Taylor,[24] J. A. Whiteway,[24] A. P. Zent[18]

The Phoenix mission investigated patterned ground and weather in the northern arctic region of Mars for 5 months starting 25 May 2008 (solar longitude between 76.5° and 148°). A shallow ice table was uncovered by the robotic arm in the center and edge of a nearby polygon at depths of 5 to 18 centimeters. In late summer, snowfall and frost blanketed the surface at night; H_2O ice and vapor constantly interacted with the soil. The soil was alkaline (pH = 7.7) and contained $CaCO_3$, aqueous minerals, and salts up to several weight percent in the indurated surface soil. Their formation likely required the presence of water.

The Phoenix mission, the first of NASA's Scout class, landed inside the arctic circle of Mars on 25 May 2008 at 23:38:24 UTC during the late northern spring. Phoenix was designed to verify the presence of subsurface H_2O ice (*1*) that was previously predicted on the basis of thermodynamic principles (*2*, *3*) and was mapped at low resolution (~500 km) within 1 m of the surface by using Odyssey's Gamma-Ray Spectrometer (GRS) instrument (*4*–*6*). Here, we address the properties of subsurface ice as well as the interaction of atmospheric water with the surface soil and the evidence that water modified this soil in the past.

Phoenix landed at 68.22°N, 234.25°E (areocentric) at an elevation of –4.1 km (referenced to Mars Orbiter Laser Altimeter areoid) on a valley floor covered by the Scandia Formation estimated to be Amazonian in age, a deposit that surrounds the northern margin of a shield volcano named Alba Patera (*7*, *8*). The Scandia Formation is interpreted as volcanic ash erupted from Alba Patera and/or as ancient polar deposits (*9*). The site also contains eroded ejecta deposits from a 10-km-diameter, bowl-shaped crater, Heimdal (fig. S1). Phoenix landed on darker ejecta deposits 20 km southwest of the crater.

The dominance of polygonal ground at the landing site (Fig. 1A) is consistent with the presence of widespread, shallow, cohesive icy soil that has undergone seasonal or longer-term freezing.

[1]Lunar and Planetary Laboratory, University of Arizona, Tucson, AZ 85721, USA. [2]Jet Propulsion Laboratory, California Institute of Technology, Pasadena, CA 91109, USA. [3]Department of Earth and Planetary Sciences, Washington University, St. Louis, MO 63130, USA. [4]Optech Incorporated, Vaughan, Ontario L4K 5Z8, Canada. [5]University of Bristol, Bristol BS8 1RJ, UK, and Department of Earth and Space Sciences, University of Washington, Seattle, WA 98195, USA. [6]Space Science Institute, Boulder, CO 80301, USA. [7]Dalhousie University, Halifax, Nova Scotia B3H 1Z9, Canada. [8]Geological Survey of Canada and University of Ottawa, Ottawa, Ontario K1A 0E8, Canada. [9]Max Planck Institute for Solar System Research, 31791 Katlenburg-Lindau, Germany. [10]Institute of Physics and Astronomy, University of Aarhus, DK-8000 Aarhus C, Denmark. [11]Canadian Space Agency, Saint-Hubert, Quebec J3Y 8Y9, Canada. [12]University of Texas–Dallas, Richardson, TX 75080, USA. [13]Tufts University, Medford, MA 02155, USA. [14]University of Alberta, Edmonton, Alberta T6G 2H1, Canada. [15]Texas A&M University, College Station, TX 77843, USA. [16]Earth and Planetary Physics, University of Copenhagen, 2100 Copenhagen, Denmark. [17]SETI Institute, Mountain View, CA 94043, USA. [18]NASA Ames Research Center, Mountain View, CA 94035, USA. [19]University of Colorado, Boulder, CO 80309, USA. [20]NASA Johnson Space Center, Houston, TX 77058, USA. [21]University of Michigan, Ann Arbor, MI 48109, USA. [22]Imperial College, London SW7 2AZ, UK. [23]Institute of Microtechnology, University of Neuchâtel, 2002 Neuchâtel, Switzerland, and Micro and Nano Engineering Laboratory, Delft University of Technology, 2628 CD Delft, Netherlands. [24]York University, Toronto, Ontario M3J 1P3, Canada.

*To whom correspondence should be addressed. E-mail: psmith@lpl.arizona.edu

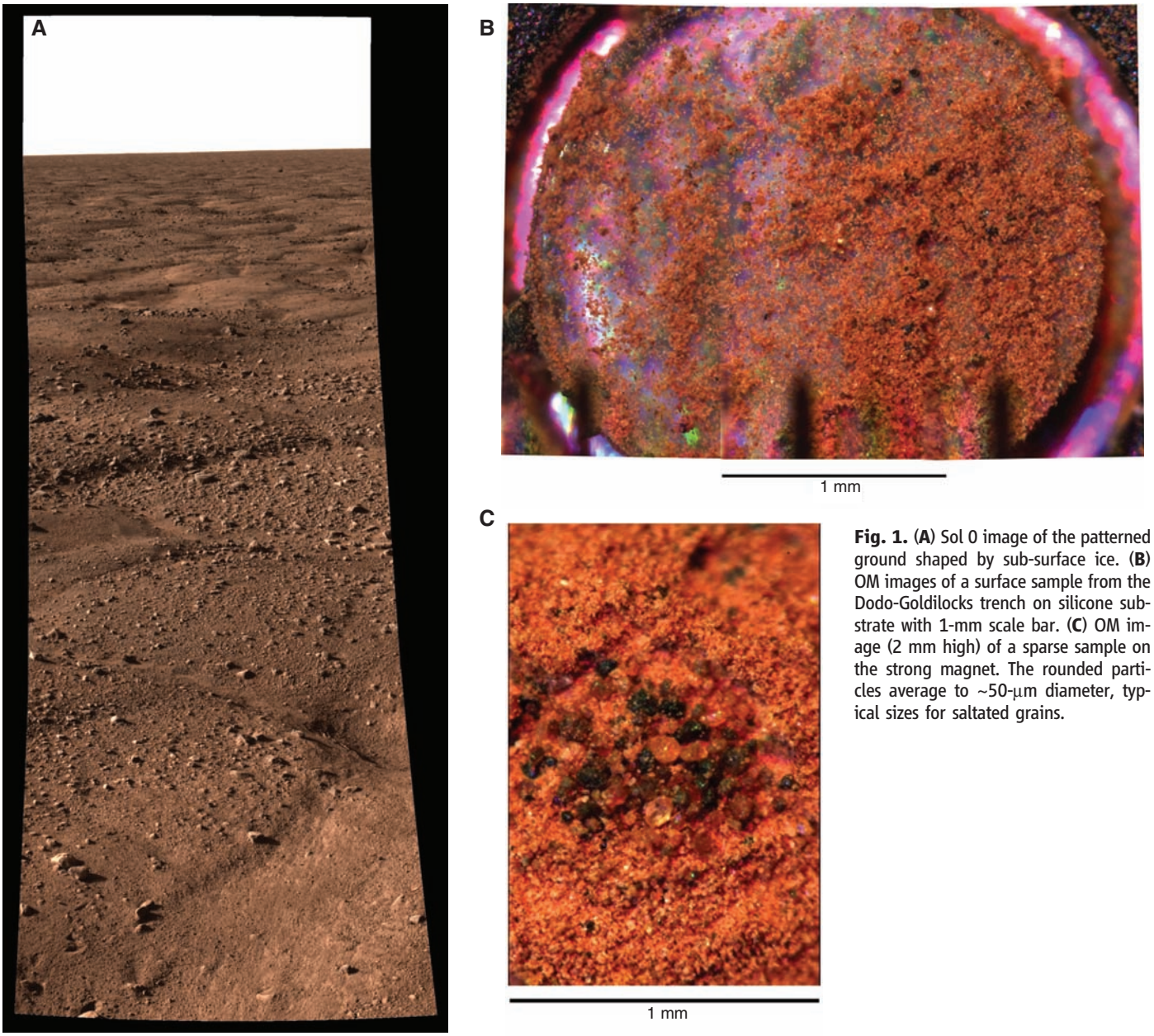

Fig. 1. (**A**) Sol 0 image of the patterned ground shaped by sub-surface ice. (**B**) OM images of a surface sample from the Dodo-Goldilocks trench on silicone substrate with 1-mm scale bar. (**C**) OM image (2 mm high) of a sparse sample on the strong magnet. The rounded particles average to ~50-μm diameter, typical sizes for saltated grains.

Contraction cracks fill with aeolian sediments and are not able to close when the icy soil warms, causing bulging of the polygon interiors (*10*). The troughs between the 2- to 3-m diameter polygons have depths of 20 to 50 cm relative to the centers. Small rocks are abundant and generally associated with troughs, but larger rocks (>1 m) are rare. A small amount of adsorbed or volumetrically bound water in the surface layer is implied by near-infrared (NIR) data from the OMEGA (Observatoire pour la Minéralogie, l'Eau, les Glaces, et l'Activité imaging spectrometer on Mars Express) and CRISM (Compact Reconnaissance Imaging Spectrometer for Mars on Mars Reconnaissance Orbiter) orbiting spectrometers at this site.

The 2.35-m Robotic Arm (RA) and associated Icy Soil Acquisition Device (ISAD) were used to excavate a dozen trenches (*11*) to the north and northeast of the lander. The upper few cm of soil is crusted, and clods were observed around the trenches and inside the RA scoop. Special procedures were developed, the "sprinkle" techniques, to reduce the clumpiness of the delivered samples.

Optical Microscope (OM) images (Fig. 1B) show particles that are the components of the soil; by number, the dominant size consists of reddish fine-grained agglomerates <10 μm across. These small particles are just under the resolution limit of the OM, but Atomic Force Microscope (AFM) imaging shows that many particles have a platy morphology (fig. S4). A second size distribution likely of different origin includes magnetic (20 to 100 μm) particles (Fig. 1C); many are black, suggesting magnetite, whereas others are brownish and less opaque. These larger particles are rounded and likely weathered by saltation. In terms of soil mass, 20% is in the reddish small particles and the other 80% in the larger particles.

The soil is likely of aeolian origin, but the crust that produces the clods formed in place. The mechanical properties are similar to those found by the Viking Lander 2 (*12*). The cloddy nature of the soil may be a consequence of cementation by carbonates (*13*) and other salts in association with small amounts of water. Because no ripples or dunes are seen, the landscape is likely deflated: Dust devils observed by Phoenix (fig. S5) scour the surface mobilizing airfall dust.

The diffusion of H_2O vapor into and out of the regolith during diurnal and seasonal cycles may produce unfrozen films of water around

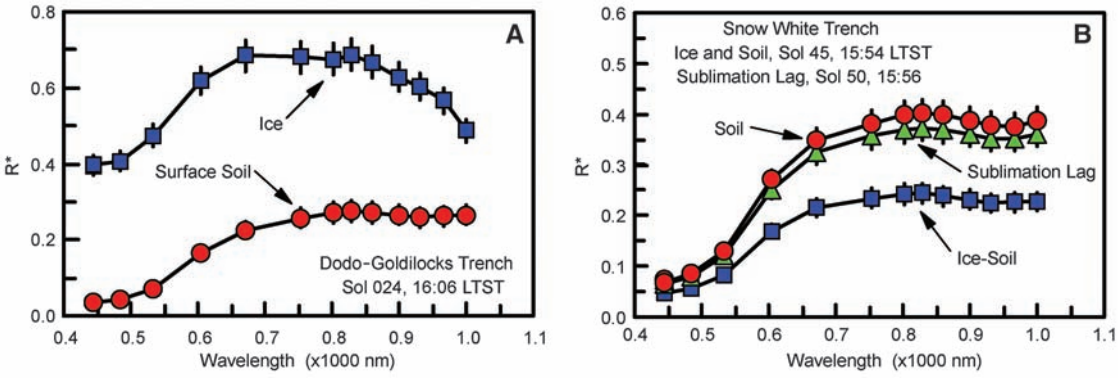

Fig. 2. Spectra reveal two different concentrations of ice mixed with soil. Error bars indicate 1σ uncertainties. (**A**) The Dodo-Goldilocks trench matches high-albedo ice with a minor soil component (<2%) compared with nearby ice-free soil exposed in the trench bottom. (**B**) The spectra in the Snow White trench correspond to low-albedo ice with a major soil component, and nearby ice-free surface soil exposed in the trench bottom and to the sublimation lag developed 5 sols later at the same location as the ice.

soil particles (*14*). The Thermal and Electrical Conductivity Probe (TECP) electrical conductivity measurements were consistent with a fully open circuit, implying that there was no effective transport of charge carriers on the scale of 15 mm. Nighttime increases in regolith dielectric permittivity, observed during the latter half of the mission (mid to late summer), imply an overnight accumulation of H_2O molecules.

A surface sample taken from the Dodo trench (fig. S8) shows two regions of water release in the Thermal and Evolved-Gas Analyzer (TEGA) oven (fig. S6, A and B): a low-temperature release from 295° to 735°C and a high-temperature release beginning near 735°C. Both indicate the presence of hydrous minerals or phases. The low-temperature region is likely indicative of phases that formed through aqueous processes. Candidate phases include iron oxyhydroxides (e.g., goethite dehydroxylation onset around 250°C), smectites (e.g., nontronite dehydroxylation onset around 300°C), kaolinite (dehydroxylation onset from 400° to 550°C depending on crystallinity), iron sulfates (e.g., jarosite dehydroxylation onset near 400°C), and magnesium sulfates (e.g, kieserite loss of crystalline water near 350°C).

The high-temperature region may reflect the presence of phases that have formed by aqueous or rock-forming processes. Candidates are smectites (e.g., montmorillonite dehydroxylation from 600° to 800°C and saponite dehydroxylation near 700° to 800°C), chlorites, talc (dehydroxylation from 750° to 850°C), serpentines (e.g., antigorite dehydroxylation from 600° to 800°C), and amphiboles (e.g., dehydroxylation near 1000°C).

TEGA has not detected low-temperature release of H_2O in the surface soils. A null detection below 295°C implies an arid soil with no adsorbed water or interstitial ice. This is unexpected because perchlorate salts (*15*) are expected to bind six to eight H_2O molecules at these cold temperatures and orbital observations detect a strong 3-μm water absorption band. TECP indicates that the soil is adsorbing water vapor at night.

Bright material was seen in one trench (Dodo-Goldilocks) at a depth of 4 to 5 cm. This material had a broad ≥1-μm absorption (*16*) and was bright in the blue filter (<0.5 μm), consistent with coarse-grained H_2O ice containing a few percent of dust

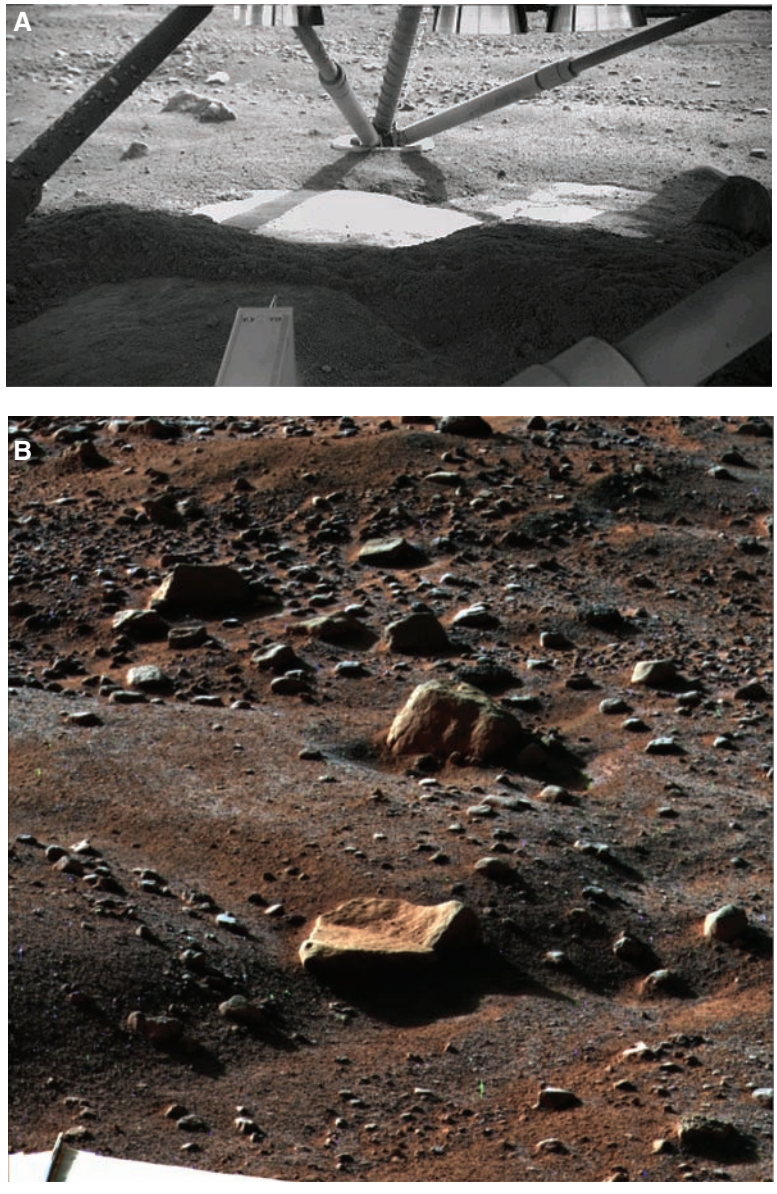

Fig. 3. (**A**) An image taken by the RA camera pointed under the lander, showing the ice table exposed by the thrusters. (**B**) Nighttime image of surface frost from sol 80 (L_s = 113°).

(Fig. 2A). Other trenches showed a weaker spectral contrast. In the Snow White trench, the ISAD scraped into a hard, icy layer that appeared to be pore ice (Fig. 2B); its albedo varied from midday to early morning (fig. S7, A and B) likely because of photometric changes in the illumination angle.

In Dodo-Goldilocks, several chunks of bright material 1.5 to 2 cm across were dislodged by the RA on sol 20 (*17*) and had disappeared by sol 24 without any obvious residue (fig. S8, A and B). This is expected for H_2O ice. Over the next 2 months, the material in the trench sublimated by several mm (fig. S8C). Pore ice has been predicted by thermodynamical arguments (*18*), but the exposure of nearly pure ice usually requires a liquid phase or brine on Earth. If dominant in the region, this supports the Odyssey GRS conclusion that ice concentrations exceed pore ice (*5*, *19*, *20*).

Because attempts to collect and to deliver ice-cemented soil materials to the TEGA ovens were not successful, we sampled sublimated till material at the bottom of one trench (Snow White) on sol 63. A small, endothermic peak was observed (fig. S9) coincident with the melting of ice with an onset temperature at –2°C and a peak around 6°C. Evolved water was recorded by TEGA's mass spectrometer as the temperature increased from –20° to +35°C.

Integration of the endothermic peak provides an estimate of the enthalpy of 0.35 J, which corresponds to 1.0 mg of water ice. If we assume that the TEGA oven was full, this sample contained ~2% ice. Because this sample was a sublimated lag, this does not represent the ice concentration in the ice layer.

Early in the mission, the RA pointed its camera under the lander to assess the footpad stability and captured an image of the ice table excavated by the 12 thrusters (Fig. 3A and fig. S3). The curved shadow of the strut provides a means to estimate its depth as 5 cm. The strut to the left of the image shows a number of blobs that have been interpreted as liquid brine splashed onto the strut during the last few seconds of landing (*21*). Perchlorate brines can have eutectic temperatures as low as –70°C once the perchlorate concentration reaches 30 to 50%. The planetary distribution of brines is unknown, if they exist at all, but salts do tend to concentrate with the presence of small amounts of water.

Atmospheric water vapor was measured regularly by using the TECP (fig. S10). Water vapor partial pressure remained near 2 Pa throughout most days, dropping rapidly at 18. local true solar time (LTST) to a minimum of <0.05 at 1.5 LTST. Vapor pressure of 2 Pa is about that of saturation over ice at 210 K. The water vapor measurements and 2-m air temperatures suggest that the typical mid-sol relative humidity was ~5%. The air was close to saturation at night early in the mission and was saturated toward the end, as seen via ground fog and low clouds (*22*). Surface temperatures are expected to be colder than those measured at 2 m, and indeed frost formation was observed in the second half of the mission (Fig. 3B).

Water ice clouds were detected by the light detection and ranging (LIDAR) (*23*) instrument as layers of enhanced back scatter. Near summer solstice, the most prominent clouds were detected at heights above 10 km. As the season progressed and the polar atmosphere cooled, clouds formed in the boundary layer in late summer [after solar longitude of Mars (L_s) = 117°], and fall streaks are clearly seen in the LIDAR observations (*22*). Late at night water ice was observed to fall from the clouds at 4 km altitude, and ground fogs were seen in the lower ~700 m of atmosphere (*22*). This diurnal cycle deposited ice onto the surface at night, reducing the vapor pressure to low values (fig. S10), sublimated it in the morning, and redistributed it throughout the planetary boundary layer in the turbulent afternoon. Near midnight, ice clouds formed and precipitated a portion of the atmospheric H_2O back to the surface in the early morning.

Orbital dynamics and particularly obliquity variations strongly influence the martian climate (*24*) and offer the possibility of liquid water in the recent past. As the obliquity exceeds 30°, the polar cap becomes warmer and increasingly unstable, releasing water vapor into the atmosphere. Models predict a wetter environment when the summer temperatures are able to exceed 0°C (*25*).

The pressure at the Phoenix landing site is always higher than the triple point pressure. Several lines of evidence support liquid films of water in the soil in the recent past: $CaCO_3$ identified by TEGA (*13*) likely forms in a wet environment, segregated ice (fig. S8, A to C) is a signature of frozen liquid water, soil is often cemented by wetted soils, and the likelihood of thicker snowfalls melting during the warmer days at high obliquity. This evidence for periodic liquid water in an alkaline environment with a sprinkling of various salts and a perchlorate energy source (*15*) implies that this region could have previously met the criteria for habitability during favorable Milankovich cycles.

References and Notes

1. P. H. Smith *et al.*, *J. Geophys. Res.* **113**, 10.1029/2008JE003083 (2008).
2. M. T. Mellon, B. M. Jakosky, *J. Geophys. Res.* **100**, 11781 (1995).
3. R. B. Leighton, B. C. Murray, *Science* **153**, 136 (1966).
4. I. G. Mitrofanov *et al.*, *Science* **300**, 2081 (2003).
5. W. V. Boynton *et al.*, *Science* **297**, 81 (2002); published online 30 May 2002 (10.1126/science.1073722).
6. W. Feldman *et al.*, *Science* **297**, 75 (2002); published online 30 May 2002 (10.1126/science.1073541).
7. R. E. Arvidson *et al.*, *J. Geophys. Res.* **113**, E00A03 (2008).
8. K. L. Tanaka, J. A. Skinner Jr., T. M. Hare, *U.S. Geol. Surv. Sci. Inv. Map (SIM) 2888* (2005).
9. K. Seelos *et al.*, *J. Geophys. Res.* **113**, E00A13 (2008).
10. M. T. Mellon *et al.*, *J. Geophys. Res.* **113**, E00A23 (2008).
11. R. Bonitz *et al.*, *J. Geophys. Res.* **113**, E00A01 (2008).
12. H. Moore *et al.*, *U.S. Geol. Surv. Prof. Pap.* 1389 (1987).
13. W. V. Boynton *et al.*, *Science* **325**, 61 (2009).
14. A. Zent, *Icarus* **196**, 385 (2008).
15. M. H. Hecht *et al.*, *Science* **325**, 64 (2009).
16. The longest wavelength filter available is at 1 μm, and the trend was downward.
17. A martian solar day has a mean period of 24 hours 39 min 35.244 s and is referred to as a sol to distinguish this from a ~3% shorter solar day on Earth.
18. M. T. Mellon *et al.*, *J. Geophys. Res.* **113**, E00A25 (2008).
19. W. C. Feldman *et al.*, *Geophys. Res. Lett.* **34**, 10.1029/2006GL028936 (2007).
20. D. A. Fisher, *Icarus* **179**, 387 (2005).
21. N. Renno *et al.*, *Lunar Planet. Sci. Conf.* **XL** (abstr. 1440) (2009).
22. J. A. Whiteway *et al.*, *Science* **325**, 68 (2009).
23. J. Whiteway *et al.*, *J. Geophys. Res.* **113**, 10.1029/2007JE003002 (2008).
24. J. A. Laskar *et al.*, *Icarus* **170**, 343 (2004).
25. R. M. Haberle, J. R. Murphy, J. Shaeffer, *Icarus* **161**, 66 (2003).

26. We thank our project manager, B. Goldstein; the Jet Propulsion Laboratory team; and our aerospace partner, Lockheed Martin. The University of Arizona supported Phoenix throughout the mission. We appreciate the help of the orbiter teams, in particular, the THEMIS (Thermal Emission Imaging System) team [P. Christensen, principal investigator (PI)] and the HiRISE (High-Resolution Imaging Science Experiment) team (A. McEwen, PI). Funding for this research came from NASA and the Canadian Space Agency.

Supporting Online Material

www.sciencemag.org/cgi/content/full/325/5936/58/DC1
Materials and Methods
Figs. S1 to S10
References

16 February 2009; accepted 1 June 2009
10.1126/science.1172339

Evidence for Calcium Carbonate at the Mars Phoenix Landing Site

W. V. Boynton,[1]* D. W. Ming,[2] S. P. Kounaves,[3] S. M. M. Young,[3]† R. E. Arvidson,[4] M. H. Hecht,[5] J. Hoffman,[6] P. B. Niles,[2] D. K. Hamara,[1] R. C. Quinn,[7] P. H. Smith,[1] B. Sutter,[10] D. C. Catling,[8,9] R. V. Morris[2]

Carbonates are generally products of aqueous processes and may hold important clues about the history of liquid water on the surface of Mars. Calcium carbonate (approximately 3 to 5 weight percent) has been identified in the soils around the Phoenix landing site by scanning calorimetry showing an endothermic transition beginning around 725°C accompanied by evolution of carbon dioxide and by the ability of the soil to buffer pH against acid addition. Based on empirical kinetics, the amount of calcium carbonate is most consistent with formation in the past by the interaction of atmospheric carbon dioxide with liquid water films on particle surfaces.

The key to understanding Mars' past climate is the study of secondary minerals that have formed by reaction with volatile compounds such as H_2O and CO_2. A wet and warmer climate during the early history of Mars, coupled with a much denser CO_2 atmosphere,